Journal of Advanced Science and Research

Contents available at: https://www.swamivivekanandauniversity.ac.in/jasr/

Nonlinear Stability Study of Capillary-Gravity Waves with Broader Bandwidth on Deep Water Using Higher-Order Formulation

Tanmoy Pal[1]

[1] *Department of Mathematics, Swami Vivekananda University, Barrackpore, West Bengal-700121, India.*

Abstract The stability characteristics of capillary-gravity waves propagating on deep water are examined through the framework of a higher-order nonlinear evolution equation de-signed to capture broader spectral bandwidth effects. By systematically incorporating higher-order dispersion and nonlinearity, the model extends beyond the classical non-linear Schrödinger equation, enabling a more accurate representation of complex wave dynamics. A linear stability analysis is conducted to investigate the modulational instability of uniform wave trains, revealing the influence of surface tension and high-order non-linear interactions on the growth rate of sideband perturbations. Numerical simulations further illustrate how capillarity modifies the instability threshold and alters the evolution patterns of wave packets. The findings provide deeper insight into the intricate interplay between gravity and capillary forces, offering refined predictive capabilities for the onset and development of instability in realistic oceanic wave conditions.

Keywords:
Nonlinear evolution equation, Capillary-gravity waves, Broader bandwidth, Modulational instability

Authors for correspondence:
Author Name: Tanmoy Pal
e-mail: tanmoypal@svu.ac.in

1. Introduction:

The nonlinear Schrödinger equation (NLSE) is frequently utilized in analyzing the nonlinear dynamics of deep-water waves due to its capability to accurately describe sideband instabilities. Typically, capillary-gravity waves arise from wind-induced shear flows near the water's surface, causing these waves to propagate within a vortical environment. Such waves significantly impact the formation and growth of wind waves, influencing ocean surface stress and consequently affecting momentum exchange between the ocean and the atmosphere. An accurate depiction of surface stress is essential for modeling and forecasting oceanic wave dynamics. Many researchers have explored the instability of finite amplitude capillary-gravity waves. Djordjevic and Redekopp [1], along with Hogan [2], analyzed cubic nonlinear envelope equations for both finite and infinite water depths, respectively, addressing the sideband instability (Benjamin-Feir instability) associated with progressive capillary-gravity waves. Dhar and Das [3] focused on a fourth-order nonlinear evolution equation (NLEE) for two interacting surface capillary-gravity waves on deep water, subsequently conducting stability analyses for uniform waves influenced by a second uniform wave. Debsarma and Das [4] derived two coupled fourth-order NLEEs that include the effects of a thin thermocline on deep-water capillary-gravity waves, subsequently reducing these coupled equations into a single equation under conditions of oblique plane wave perturbations to analyze uniform wave stability. Trulsen and Dysthe [5] formulated a higher-order NLEE to describe broader bandwidth surface gravity waves on deep water, explicitly considering wave bandwidth and nonlinearity scales as O(ϵ^(1/2)) and O(ϵ), respectively. Adopting the scaling framework introduced by Trulsen and Dysthe [5], finite depth, deep water, and infinite depth scenarios correspond to (kh)^(-1) being O(1),O(ϵ), and 0, respectively.

This paper expands on Trulsen and Dysthe's [5] methodology by integrating capillary effects. The primary objective is to derive an advanced higher-order NLEE applicable to broader bandwidth conditions and formulate a weakly nonlinear theoretical model for capillary-gravity waves in deep water.

2. The Governing Equations and The Fourth-order Evolution Equation

The governing equations for surface capillary-gravity waves in an inviscid, incompressible, and irrotational fluid of uniform depth are formulated as follows:

$$\nabla^2\phi = 0 \quad \text{for} \quad -h < z < \eta(x,y,t) \tag{1}$$

where $\phi(x,y,z,t)$ denotes the velocity potential of the fluid.

At the free surface $z = \eta$, the kinematic boundary condition is expressed by

$$\phi_z - \eta_t = \phi_x\eta_x + \phi_y\eta_y \quad \text{at} \quad z = \eta \tag{2}$$

The dynamic boundary condition at $z = \eta$ incorporates both gravitational and capillary effects, written as

$$\phi_t + \eta = -\frac{1}{2}(\nabla\phi)^2 + \kappa\frac{\eta_{xx}+\eta_{yy}+\eta_x^2\eta_{xx}-2\eta_x\eta_y\eta_{xy}+\eta_y^2\eta_{yy}}{(1+\eta_x^2+\eta_y^2)^{3/2}} \tag{3}$$

At the rigid bottom $z = -h$, the impermeability condition is

$$\phi_z = 0, \quad z = -h \tag{4}$$

Here, $\phi(x,y,z,t)$ represents the velocity potential and $\eta(x,y,t)$ denotes the free surface displacement. ρ is the fluid density, g is the gravitational acceleration, and T is the surface tension coefficient. The gradient operator is given by

$$\nabla = \left(\frac{\partial}{\partial x}, \frac{\partial}{\partial y}, \frac{\partial}{\partial z}\right).$$

The system is non-dimensionalized through the following transformations:

$$\tilde{\phi} = \frac{k_0^3}{g}\phi, \quad \tilde{\eta} = k_0\eta, \quad (\tilde{x},\tilde{y},\tilde{z}) = (k_0x, k_0y, k_0z), \quad \tilde{t} = \omega t, \quad \kappa = \frac{Tk_0^2}{\rho g} \tag{5}$$

where k_0 is a reference wavenumber, ω is the characteristic frequency, and κ quantifies the effect of surface tension. For simplicity, tildes are omitted in the remaining expressions.

The general solution of the above equations can be decomposed as

$$B = \bar{B} + \sum_{p=1}^{\infty}\left[B_p \exp\{ip(kx - \omega t)\} + \text{c.c.}\right] \tag{6}$$

where B denotes either ϕ or ζ, B_p are the harmonic amplitudes, k and ω represent the wavenumber and frequency of the primary wave, and c.c. indicates complex conjugate terms.

The slow modulation of wave amplitudes is described by the slow drift term $\bar{\phi}$ and the harmonic components ϕ_p, η_p, which depend on the slow spatial variables $\epsilon x, \epsilon y, \epsilon z$ and slow time ϵt, with ϵ being a small parameter indicating weak nonlinearity. We focus on the fourth-order nonlinear evolution equation (NLEE) applicable for waves with a broad spectral bandwidth under weakly nonlinear conditions. The scaling assumptions are

$$k_0a = O(\epsilon), \quad \frac{|\kappa|}{k_0} = O(\epsilon), \quad (k_0h)^{-1} = O(\epsilon) \tag{7}$$

The linear dispersion relation for the primary wave mode ($l = 0$) is given by

$$f(\omega,k,l) = \omega - \sqrt{k^2 + \kappa[1 + (k^2 + l^2)]^2} = 0 \tag{8}$$

where ω and k denote the frequency and wavenumber of the carrier wave, respectively.

By employing the standard analytical technique developed by Dhar and Das [6], we derive the fourth-order coupled NLEEs governing the free surface displacement ζ, where $\eta = \eta_{11} + \epsilon\eta_{12}$, and the mean flow component $\bar{\phi}$ is described as

$$i\left(\frac{\partial\eta}{\partial\tau} + c_g\frac{\partial\eta}{\partial x}\right) - \gamma_1\frac{\partial^2\eta}{\partial x^2} + \gamma_2\frac{\partial^2\eta}{\partial y^2} + i\left(\gamma_3\frac{\partial^3\eta}{\partial x^3} + \gamma_4\frac{\partial^3\eta}{\partial x\,\partial y^2}\right) = \mu_1|\eta|^2\eta^* + i\left(\mu_2|\zeta|^2\frac{\partial\eta}{\partial x} + \mu_3\eta^2\frac{\partial\eta^*}{\partial x}\right) + \eta\frac{\partial\bar{\phi}}{\partial x} \tag{9}$$

The equation for the slow potential $\bar{\phi}$ satisfies Laplace's equation within the fluid domain:

$$\nabla^2\bar{\phi} = 0, \quad \text{for} \quad -h < z < 0 \tag{10}$$

At the free surface $z = 0$, the vertical derivative of $\bar{\phi}$ is related to the surface elevation by

$$\frac{\partial\bar{\phi}}{\partial z} = 2\frac{\partial}{\partial x}(|\eta|^2), \quad z = 0 \tag{11}$$

At the bottom boundary $z = -h$, the vertical derivative of $\bar{\phi}$ vanishes:

$$\frac{\partial\bar{\phi}}{\partial z} = 0, \quad z = -h \tag{12}$$

When $\kappa = 0$, equation (9) reduces exactly to equation (10) found in the work of Trulsen and Dysthe [5]. Generally, it is assumed that both wave steepness and spectral bandwidth are of the same order, $O(\epsilon)$, allowing the nonlinear and dispersive effects to balance at the fourth-order level, corresponding to $O(\epsilon^4)$.

3. Stability Analysis:

A uniform wave train solution to NLEEs is expressed as

$$\eta = \frac{\eta_0}{2}e^{-i\mu_1\eta_0^2 t/4}, \bar{\phi} = \phi_0, \tag{13}$$

where η_0, ϕ_0 are real constants.

Next, we introduce small perturbations on this uniform wave train, written as

$$\eta = \frac{\eta_0}{2}(1+\eta')e^{i(\theta'-\Delta\omega t)}, \ \bar{\phi} = \phi_0(1+\phi'), \tag{14}$$

where η', θ' denote small amplitude and phase perturbations, and ϕ' represents a small fluctuation in $\bar{\phi}$. By substituting expression (14) into equation (9), we obtain a system of two linearized equations in terms of η' and θ'. We then consider plane wave solutions of these perturbations, given by

$$\begin{pmatrix}\eta'\\ \theta'\end{pmatrix} = \begin{pmatrix}\hat{\eta}\\ \hat{\theta}\end{pmatrix}e^{i(\lambda x+\mu y-\Omega t)} + c.c. \tag{15}$$

$$\phi' = \hat{\phi}\left\{e^{i(\lambda x+\mu y-\Omega t)} + c.c.\right\}\frac{\cos\bar{k}(z+h)}{\cosh(\bar{k}h)}, \ \bar{k}^2 = \lambda^2+\mu^2, \tag{16}$$

Here, λ, μ are the perturbation wavenumbers and Ω is the perturbed frequency, which are related through the following nonlinear dispersion relation:

$$\left\{\bar{S_1} + \frac{(\mu_2+\mu_3)}{4}\eta_0^2\lambda\right\}\left\{\bar{S_1} + \frac{(\mu_2-\mu_3)}{4}\eta_0^2\lambda\right\} = \bar{S_2}\left\{\bar{S_2} - \frac{\mu_1}{2}\eta_0^2 + \frac{\lambda^2\eta_0^2}{\bar{k}\tanh(\bar{k}h)}\right\}, \tag{17}$$

where $\bar{S_1} = \Omega - c_g\lambda + \gamma_3\lambda^3 + \gamma_4\lambda\mu^2$ and $\bar{S_2} = \gamma_1\lambda^2 - \gamma_2\mu^2$ and c_g represents the group velocity of the carrier wave.

Solving equation (17) leads to

$$\bar{S_1} = -\frac{\mu_2}{4}\eta_0^2\lambda \pm \sqrt{\bar{S_2}\left\{\bar{S_2} - \frac{\mu_1}{2}\eta_0^2 + \frac{\lambda^2\eta_0^2}{\bar{k}\tanh(\bar{k}h)}\right\}} \tag{18}$$

From equation (18), instability occurs if

$$\bar{S_2}\left\{\bar{S_2} - \frac{\mu_1}{2}\eta_0^2 + \frac{\lambda^2\eta_0^2}{\bar{k}\tanh(\bar{k}h)}\right\} < 0 \tag{19}$$

Whenever condition (19) holds, the perturbed frequency Ω becomes complex, and the corresponding instability growth rate is determined by the imaginary component Ω_i , given by

$$\Omega_i = \sqrt{(\gamma_1\lambda^2 - \gamma_2\mu^2)\left(\frac{\mu_1}{2}\eta_0^2 - \gamma_1\lambda^2 + \gamma_2\mu^2 - \frac{\lambda^2\eta_0^2}{\bar{k}\tanh(\bar{k}h)}\right)}. \tag{20}$$

4. Higher-order Evolution Equation for Broader Bandwidth

To achieve improved spectral resolution, we follow the approach of Trulsen and Dysthe [5] and apply the following scaling relations:

$$k_0A = O(\epsilon), \quad \frac{|\kappa|}{k_0} = O(\epsilon^{1/2}), \quad (k_0h)^{-1} = O(\epsilon^{1/2}) \tag{21}$$

Here, we utilize similar harmonic expansions, as in (6), for the velocity potential ϕ and the free surface elevation η. In this context, $\phi_p, \eta_p, \bar{\phi}, \eta_0$ (for $p = 1,2, ...$) are now dependent on the slowly varying modulation variables $\epsilon^{1/2}t, \epsilon^{1/2}x, \epsilon^{1/2}y$, while $\bar{\phi}$ also evolves over a slightly faster scale characterized by $\epsilon^{1/2}$.

Next, we expand the perturbations using the following series:

$$E_1 = \sum_p \epsilon^{p/2} E_{1p}, \quad E_2 = \sum_p \epsilon^{p/2} E_{2p} \tag{22}$$

where E_j represents B_j and ζ_j, and $B_j = (\phi_j, \eta_j), \quad j = 1,2.$

In this formulation, we maintain the same order of nonlinearity as in equation (9) but exclude quartic nonlinear terms, meaning all fourth-order contributions are neglected. This justifies constructing the new evolution equation for broader bandwidth limited to order $O(\epsilon^{7/2})$.

Following the perturbation procedure similar to Dhar and Das [6], we ultimately derive the coupled nonlinear evolution equations (NLEEs) for broader bandwidth as

$$i\left(\frac{\partial \eta}{\partial \tau} + c_g \frac{\partial \eta}{\partial x}\right) - \gamma_1 \frac{\partial^2 \eta}{\partial x^2} + \gamma_2 \frac{\partial^2 \eta}{\partial y^2} + i\left(\gamma_3 \frac{\partial^3 \eta}{\partial x^3} + \gamma_4 \frac{\partial^3 \eta}{\partial x\, \partial y^2}\right)$$

$$+\gamma_5 \frac{\partial^4 \eta}{\partial x^4} + \gamma_6 \frac{\partial^4 \eta}{\partial x^2\, \partial y^2} + \gamma_7 \frac{\partial^4 \eta}{\partial x^3\, \partial y} + \gamma_8 \frac{\partial^4 \eta}{\partial x\, \partial y^3}$$

$$+i\left(\gamma_9 \frac{\partial^5 \eta}{\partial x^5} + \gamma_{10} \frac{\partial^5 \eta}{\partial x^3\, \partial y^2}\right) = \mu_1 |\eta|^2 \eta^* + i\left(\mu_2 |\eta|^2 \frac{\partial \eta}{\partial x} + \mu_3 \eta^2 \frac{\partial \eta^*}{\partial x}\right) + \eta \frac{\partial \bar{\phi}}{\partial x} \tag{23}$$

The governing equation for $\bar{\phi}$ is

$$\nabla^2 \bar{\phi} = 0, \quad -h < z < 0 \tag{24}$$

At the free surface $z = 0$, the vertical derivative of $\bar{\phi}$ satisfies

$$\frac{\partial \bar{\phi}}{\partial z} = 2 \frac{\partial}{\partial x}(|\eta|^2), \quad z = 0 \tag{25}$$

And at the bottom boundary $z = -h$:

$$\frac{\partial \bar{\phi}}{\partial z} = 0, \quad z = -h \tag{26}$$

The coefficients γ_i, μ_i used in these equations are detailed in the Appendix.

In this broader bandwidth NLEE, we assume the wave steepness scales as $O(\epsilon)$, while the bandwidth expands at $O(\epsilon^{1/2})$, ensuring the nonlinear and dispersive terms balance at $O(\epsilon^{7/2})$.

In the absence of capillarity, the equation (23) reduces to an equation (21) of Trulsen and Dysthe [5].

Proceeding as in section 3, we obtain the nonlinear dispersion relation as follows

$$\left\{R_1 + \frac{(\mu_2+\mu_3)}{4}\eta_0^2\lambda\right\}\left\{R_1 + \frac{(\mu_2-\mu_3)}{4}\eta_0^2\lambda\right\} = R_2\left\{R_2 - \frac{\mu_1}{2}\eta_0^2 + \frac{\lambda^2\eta_0^2}{\bar{k}\tanh(\bar{k}h)}\right\}, \tag{27}$$

where

$$R_1 = \Omega - c_g\lambda + \gamma_3\lambda^3 + \gamma_4\lambda\mu^2 - \gamma_8\lambda^5 - \gamma_9\lambda^3\mu^2 - \gamma_{10}\lambda\mu^4, \tag{28}$$

$$R_2 = \gamma_1\lambda^2 - \gamma_2\mu^2 + \gamma_5\lambda^4 + \gamma_6\lambda^2\mu^2 + \gamma_7\mu^4. \tag{29}$$

The solution of (27) is given by

$$R_1 = -\frac{\mu_2}{4}\eta_0^2\lambda \pm \sqrt{R_2\left\{R_2 - \frac{\mu_1}{2}\eta_0^2 + \frac{\lambda^2\eta_0^2}{\bar{k}\tanh(\bar{k}h)}\right\}} \tag{30}$$

Using (28) the equation (27) can be expressed as

$$\Omega = c_g\lambda - \gamma_3\lambda^3 - \gamma_4\lambda\mu^2 + \gamma_8\lambda^5 + \gamma_9\lambda^3\mu^2 + \gamma_{10}\lambda\mu^4 - \frac{\mu_2}{4}\zeta_0^2\lambda \pm \sqrt{R_2\left\{R_2 - \frac{\mu_1}{2}\zeta_0^2 + \frac{\lambda^2\zeta_0^2}{\bar{k}\tanh(\bar{k}h)}\right\}} \tag{31}$$

If we set $\kappa = 0$, then the equation (31) reduces to an equation equivalent to equation (25) of Trulsen and Dysthe [5].

It follows from (31) that for instability we have

$$R_2\left\{R_2 - \frac{\mu_1}{2}\eta_0^2 + \frac{\lambda^2\eta_0^2}{\bar{k}\tanh(\bar{k}h)}\right\} < 0 \tag{32}$$

The instability growth rate Ω_i, which is the imaginary part of the perturbed frequency Ω, is given by

$$\Omega_i = \sqrt{R_2\left(\frac{\mu_1}{2}\eta_0^2 - R_2 - \frac{\lambda^2\eta_0^2}{\bar{k}\tanh(\bar{k}h)}\right)} \tag{33}$$

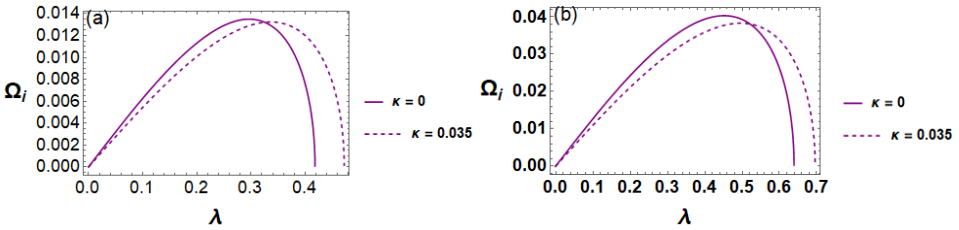

Fig-1: Plot of growth rate of instability Ω_i against λ for $h = 6$ and two values of ; (a) $\eta_0 = 0.2$, (b) $\eta_0 = 0.4$.

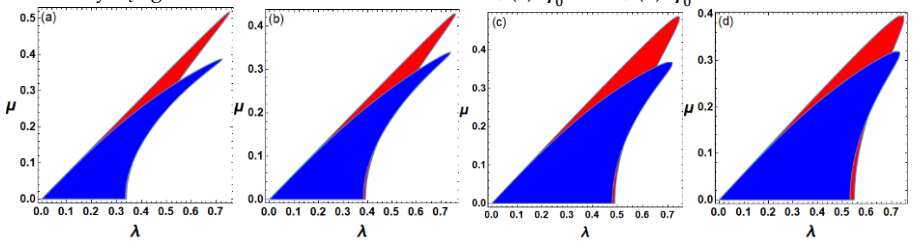

Fig-2: The (λ, μ) instability diagrams for $h = 6$; (a) $\kappa = 0, \eta_0 = 0.15$, (b) $\kappa = 0.035, \eta_0 = 0.15$, (c) $\kappa = 0, \eta_0 = 0.25$, (d) $\kappa = 0.035, \eta_0 = 0.25$; Blue regions corresponding to new broader-banded result and red regions to narrow-banded result.

The graphical representation of the instability growth rate (GRI), denoted by Ω_i and calculated from equation (33), is presented in Fig. 1. This plot shows the variation of Ω_i with respect to λ for the broader bandwidth case, considering $h = 6$ along with different values of the capillarity parameter κ and wave steepness η_0.

It is observed that capillary effects lead to a noticeable reduction in the instability growth rate, thereby exerting a stabilizing effect on the system. Furthermore, the GRI exhibits a significant increase as the wave steepness η_0 becomes larger.

According to the instability criterion derived in equation (32), the corresponding modulational instability zones in the (λ, μ) plane are displayed in Fig. 2 for two specific values of wave steepness, namely $\eta_0 = 0.15$ and $\eta_0 = 0.25$, along with $\kappa = 0$ and $\kappa = 0.035$. From these results, it is evident that both capillarity and wave steepness play a significant role in altering the characteristics and extent of the instability regions.

5. Numerical validation

We employ the Chebyshev spectral collocation method combined with Fourier techniques to numerically investigate the dynamics of surface capillary-gravity waves governed by the Laplace equation with nonlinear free-surface boundary conditions. Time integration is performed using a fourth-order Runge-Kutta scheme, ensuring stability and accuracy in the temporal evolution. The numerical simulations reveal the significant influence of capillarity on wave dynamics, demonstrating an increase in wave frequency with higher surface tension coefficients. Additionally, time-evolution studies of surface profiles highlight the transition from gravity-dominated slow oscillations to capillarity-dominated high-frequency, rapidly decaying waves. Modulational instability analysis confirms that capillarity enhances the growth rate of perturbations, leading to faster amplification of sideband modes. Spectral energy distribution further indicates a pronounced nonlinear energy transfer toward higher harmonics in the presence of strong capillarity. Overall, this numerical framework provides a robust approach to capturing both the dispersive and modulational characteristics of surface capillary-gravity waves.

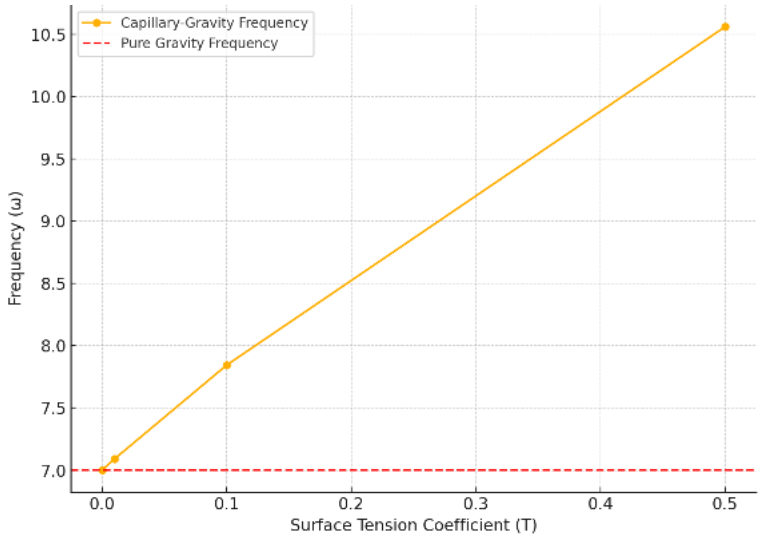

Fig-3: Effect of capillary on wave frequency.

Fig.3 illustrates the relationship between the wave frequency ω and the surface tension coefficient T, highlighting the impact of capillarity on wave dynamics. It is observed that as the value of T increases, there is a marked increase in the corresponding wave frequency ω. In the absence of capillary effects, i.e., when T=0, the frequency closely follows the theoretical prediction for pure gravity waves, where surface tension does not influence wave propagation. However, with the introduction and gradual increase of capillarity, the wave frequency rises substantially, deviating from the gravity wave prediction. This effect becomes particularly prominent in the regime of short wavelengths, corresponding to higher wavenumbers k. For these shorter waves, surface tension exerts a dominant force, resulting in a significant elevation of frequency. The graph effectively demonstrates that capillary forces play a crucial role in modifying wave characteristics, especially at smaller scales where their influence is more pronounced.

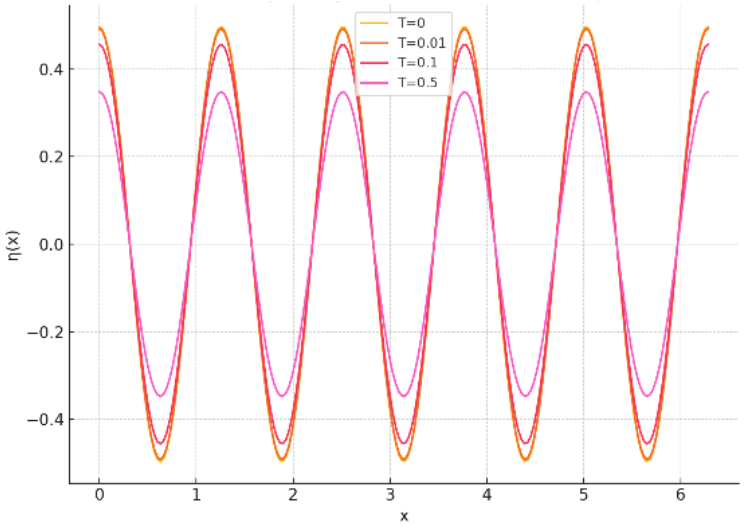

Fig-4: Effect of capillary on surface profile.

The influence of surface tension on the evolution of the surface wave profile is shown in Fig. 4. As the surface tension coefficient T increases, the damping effect on wave amplitude becomes more pronounced, leading to a more rapid attenuation of wave height over time. Elevated surface tension contributes to a smoother wave surface by significantly reducing the peak amplitudes of oscillations. Furthermore, the enhanced capillarity acts to suppress smaller-scale surface disturbances, effectively stabilizing short-wavelength undulations. This stabilization promotes the formation of smoother profiles characterized by higher-frequency, less energetic wave motions. Overall, increasing Tnot only diminishes the energy of surface waves but also alters the dominant frequency characteristics, favoring a more uniform and refined surface structure.

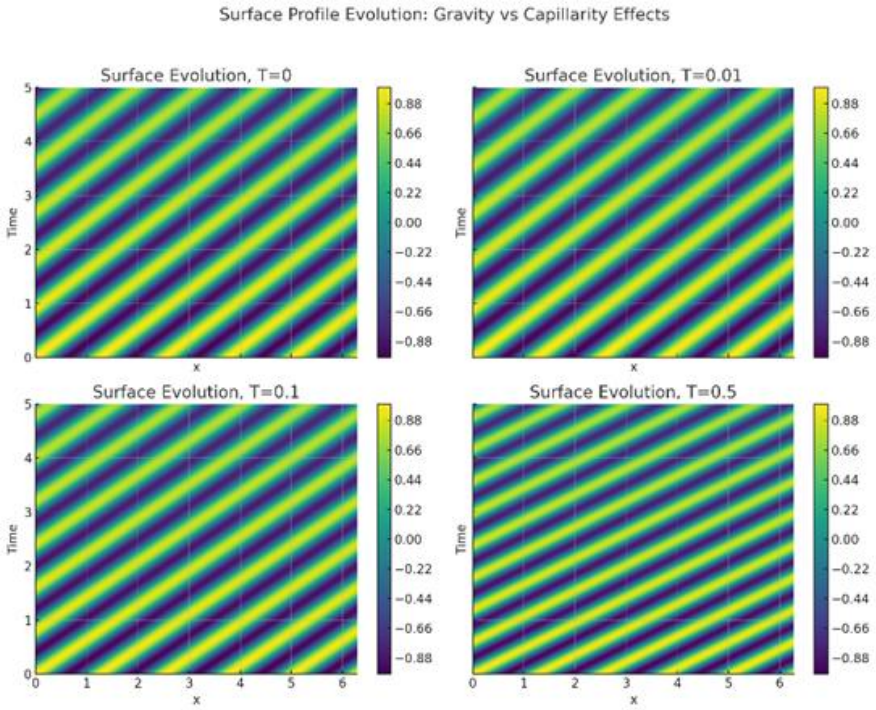

Fig-5: Surface profile evolution for $T = 0, 0.01, 0.1, 0.5$.

Fig. 5 illustrates the evolution of the surface wave profile under varying effects of capillarity. In the top-left panel, where the surface tension parameter $T = 0$, the wave behavior is governed purely by gravity, resulting in slower oscillations with relatively large amplitudes and gradual temporal evolution. Introducing a slight capillary influence at $T = 0.01$ (top-right) leads to a subtle increase in oscillation frequency accompanied by a modest reduction in wave amplitude, indicating the initial onset of capillarity effects. As the capillary contribution becomes more pronounced at $T = 0.1$ (bottom-left), the wave frequency increases more noticeably and the amplitude decays at a faster rate, suggesting a significant interaction between gravitational and capillary forces. Finally, in the bottom-right panel with $T = 0.5$, the system is dominated by capillarity, characterized by rapid high-frequency oscillations and a swift reduction in amplitude, clearly depicting the transition to a capillarity-dominant wave regime.

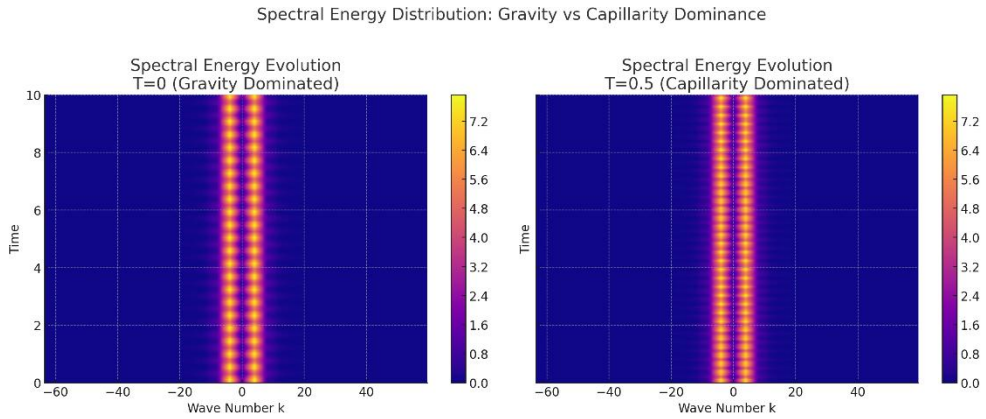

Fig-5: Spectral energy distribution for $T = 0,\ 0.5$.

Figure 6 illustrates the contrasting energy distribution patterns for two distinct regimes of wave dynamics. In the left panel, corresponding to $T = 0$, where gravitational effects dominate, the spectral energy remains primarily localized around the initial carrier wavenumber k. This reflects a narrow-banded wave evolution with minimal energy transfer to higher harmonics, indicating weak nonlinear interactions and stable wave propagation. In contrast, the right panel, representing $T = 0.5$ with capillarity as the dominant force, reveals a significant redistribution of energy towards higher wavenumbers. A rapid and extensive energy transfer is observed, characterized by a pronounced excitation of multiple harmonic modes. This behavior highlights the presence of strong nonlinear energy cascades and enhanced wave interactions, leading to notable spectral broadening. The comparison clearly demonstrates how capillarity intensifies the complexity of wave dynamics by promoting broader spectral energy spread and facilitating more vigorous nonlinear wave interactions.

6. Conclusions

This study focuses on a modified NLEE tailored for broader bandwidth capillary-gravity waves on deep water. The incorporation of additional linear terms within the modified NLEE significantly improves the spectral bandwidth resolution. This enhancement helps overcome a primary limitation associated with conventional band-restricted NLEE models, making the newly derived equation more suitable for numerical simulations of weakly nonlinear surface waves. Using this improved NLEE, the range of instability regions is notably reduced. The instability analysis of uniform wave trains derived from the broader-band formulation shows improved accuracy compared to narrow-band approaches and closely aligns with the exact outcomes reported by Mclean et al. [7] in cases without capillarity effects. Consequently, the present equation, offering adequate spectral width, is anticipated to be highly effective for practical ocean wave applications. Future research could involve generating contour plots of the growth rate index (GRI) in the (λ,μ) plane for both finite and infinite water depths, as well as exploring how instability regions and peak GRI vary with wave steepness in infinite depth scenarios.

Appendix

$$\gamma_1 = \frac{B}{2\sigma h_\sigma^2(1+\kappa)}, \gamma_2 = \frac{1+3\kappa}{\sigma h_\sigma^2}, \gamma_3 = \frac{2AB-\kappa h_\sigma^4}{2\sigma h_\sigma^4(1+\kappa)}, \gamma_4 = \frac{(1-3\kappa)h_\sigma^2-2(1+3\kappa)A}{4\sigma h_\sigma^2(1+\kappa)},$$

$$\gamma_5 = \frac{A^4+4A^2B-6A^2\kappa h_\sigma^2-2A\kappa h_\sigma^4+9\kappa^2 h_\sigma^2}{2\sigma h_\sigma^6(1+\kappa)}, \gamma_6 = \frac{(1-3\kappa)Ah_\sigma^2-(1+3\kappa)\left(2A^2+B\right)-\{(h_\sigma\}^4/2)}{2\sigma h_\sigma^4(1+\kappa)},$$

$$\gamma_7 = \frac{2(1+3\kappa)^2+(1-3\kappa)h_\sigma^2}{16\sigma h_\sigma^2(1+\kappa)}, \gamma_8 = \frac{-2AB\left(4A^2+3B\right)+4B\kappa h_\sigma^4+4uA\kappa h_\sigma^5+2\{h_k^2-\left(u^2-3\kappa\right)h_\sigma^2\}\kappa h_\sigma^4}{2\sigma h_\sigma^8(1+\kappa)},$$

$$\gamma_9 = \frac{(1+3\kappa)\left(4A^3+6AB-\kappa h_\sigma^4\right)-(1-3\kappa)\left(2A^2h_\sigma^2+Bh_\sigma^2\right)+Ah_\sigma^4-\{(h_\sigma\}^6/2)}{2\sigma h_\sigma^6(1+\kappa)},$$

$$\gamma_{10} = \frac{-2(1-3\kappa)Ah_\sigma^2-12(1+3\kappa)^2A+4(1+3\kappa)(1-3\kappa)h_\sigma^2+3(1-\kappa)h_\sigma^4}{16\sigma h_\sigma^4(1+\kappa)}, \mu_1 = \frac{1}{\sigma h_\sigma^2}\left\{\frac{4(1+\kappa)(2-\kappa)}{1-2\kappa}-3\kappa\right\}$$

$$\mu_2 = \frac{3\left(4\kappa^4+4\kappa^3-9\kappa^2+\kappa-8\right)}{\sigma h_\sigma^2(1+\kappa)(1-2\kappa)^2}, \mu_3 = \frac{\left(2\kappa^2+\kappa+8\right)(1-\kappa)}{2\sigma h_\sigma^2(1+\kappa)(1-2\kappa)}, A = f_k, B = {f_k}^2 - 3\kappa f_\sigma^2, f_k = \frac{\partial f}{\partial k}, f_\sigma = \frac{\partial f}{\partial \sigma}.$$

References

1. Djordjevic, V. D. and Redekopp, L. G., "On two-dimensional packets of capillary-gravity waves", Journal of Fluid Mechanics 79(4), 703-714 (1977).

2. Hogan, S. J., "The fourth-order evolution equation for deep-water gravity-capillary waves", Proc. R. Soc. Lond. A402, 359–372 (1985).

3. Dhar, A. K. and Das, K. P., "Effect of capillarity on fourth-order nonlinear evolution equations for two Stokes wave trains in deep water", J. Indian Inst. Sci. 73, 579 (1993).

4. Debsarma, S. and Das, K. P., "Fourth order nonlinear evolution equations for gravity-capillary waves in the presence of a thin thermocline in deep water", The Anziam Journal 43(4), 513-524 (2002).

5. Trulsen, K. and Dysthe, K. B., "A modified nonlinear Schrödinger equation for broader bandwidth gravity waves on deep water", Wave Motion 24(3), 281-289 (1996).

6. Dhar, A. K. and Das, K. P., "A fourth-order evolution equation for deep water surface gravity waves in the presence of wind blowing over water", Physics of Fluids A: Fluid Dynamics 2, no. 5,778–783 (1990).

7. McLean, J. W., Ma, Y. C., Martin, D. U., Saffman, P. G. and Yuen, H. C. "Three-dimensional in-stability of finite-amplitude water waves", Phys. Rev. Lett. 46: 817–820 (1981).